Three-dimensional simulation of a pair of vertical-axis wind turbines with a longitudinal arrangement in urban environments: An analysis of wake characteristics and power output

Lin Wen[1], Xiulan Ye[1] and Xuelin Zhang[1,2,3]

[1] School of Atmospheric Sciences, Sun Yat-sen University, and Southern Marine Science and Engineering Guangdong Laboratory (Zhuhai), Zhuhai, People's Republic of China

[2] Key Laboratory of Tropical Atmosphere-Ocean System (Sun Yat-sen University), Zhuhai, People's Republic of China

[3] Guangdong Province Key Laboratory for Climate Change and Natural Disaster Studies, Sun Yat-sen University, Zhuhai, People's Republic of China

ABSTRACT

Vertical-axis wind turbines are often used to capture wind energy in urban environments. The arrangements of vertical-axis wind turbines have important effects on the recovery of wind energy and power generation. The longitudinal arrangement is a common element in wind turbine arrays but has been explored less in previous studies. This analysis simulated a pair of vertical-axis wind turbines with a longitudinal arrangement under three-dimensional (3D) simulation. It analysed the wake characteristics and power output by setting the two layouts of C-C and CO-C for two turbines. The results revealed that the maximum wake deficit of C-C is about 10% larger than that of CO-C due to the wake superposition effect in the same direction. The wake velocity in both the C-C and CO-C cases can recover by 80% at a downstream distance of 5.5D behind the turbines, which is also a suitable distance to place the additional turbine. The Coefficient of Power (Cp) of C-C is larger than that of CO-C, which means that the layout of C-C should be prioritised in the longitudinal arrangement.

KEYWORDS Wind energy; urban environment; sustainable development; wind turbine layout; renewable energy
CONTACT Xuelin Zhang zhangxlin25@mail.sysu.edu.cn
Received 22 November 2024

1. Introduction

With the growing development of urbanisation and substantial changes occurring in the urban wind and thermal environment, sustainable growth in urban areas has emerged as a hot issue in the last few years (Toja-Silva et al., 2013). Urban wind energy, a renewable energy that can be developed in cities, has gradually attracted much attention from scholars and holds large potential for future research in urban environments (Škvorc and Kozmar, 2021).

Vertical-axis wind turbines are often used to capture city wind energy (Figure 1). They can better adapt to the complex turbulent flow field and various wind direction conditions in urban environments in comparison with horizontal-axis wind turbines (Rezaeiha et al., 2020). These turbines are often installed on rooftops (Huang et al., 2017), building walls (Xu et al., 2021a), between buildings (Juan et al., 2022; Zhou et al., 2017), or inside ventilation ducts (Hassanli et al., 2017) to harvest wind energy. In previous studies, researchers usually studied urban wind energy by altering the building layouts and the positions of turbines (Abohela et al., 2013; Balduzzi et al., 2012) to find the most suitable arrangement of wind turbines at the microscale.

The arrangement of wind turbines and the parameter design of wind turbines also significantly affect wind energy harvesting. Previous studies have made a deep exploration of single wind turbine by conducting a series of studies concerning various design parameters, including tip speed ratio, number of blades, azimuth angle, airfoil shape, and others (Raciti Castelli et al., 2011; Rezaeiha et al., 2018), to study their influence on the power output and aerodynamic performance. Similarly, the arrangement of multiple wind turbines also has been investigated to analyse the aerodynamic performance. In these studies, a pair of two turbines is the most common subject of research, and there are usually three aspects for study: the lateral arrangement, the longitudinal arrangement, and their combinations. Because a pair of wind turbines is a basic and important element in wind turbine arrays, compared with the complex movement of turbine arrays, the study of a pair of turbines is representative, which can help us gain a better understanding of the turbines' movement from the micro level and discover a new perspective for the future design of multiple wind turbines.

Many studies have deeply analysed the motion characteristics of a pair of wind turbines with the lateral arrangement (Zanforlin and Nishino, 2016). For example, Lam and Peng (2017) studied two wind turbines with a fixed lateral distance and analysed their wake characteristics and the distribution of velocity fields under the conditions of a rotating clockwise or counterclockwise direction; Zanforlin and Nishino (2016) applied the Computational Fluid Dynamics (CFD) simulation, studied the movement

(a) (b) (c)

Figure 1. Examples of application scenarios of vertical-axis wind turbines in urban environments.

of two wind turbines placed closely and their influence on the enhancement of the wind power generation; Müller et al. (2021) detailedly studied the wake recovery behind the two wind turbines from the two aspects of vertical distribution and horizontal distribution. However, for the longitudinal arrangement, fewer studies have discussed the interactions between the two turbines due to the commonly held belief that it generates lower overall power (Brownstein et al., 2016). Xu et al. (2021a) studied the power generation of turbine arrays that consist of five rows and 10 columns of wind turbines put in two buildings. Still, the study focused on the interaction between the turbines in the same row. Therefore, it is essential to further explore wind turbines with the longitudinal arrangement (Brownstein et al., 2016). The capacity of this arrangement should receive more attention and development (Xu et al., 2021b). By analysing this, we can better understand the patterns of urban wind energy output from turbine arrays and maximise wind energy utilisation.

There are two methods of CFD simulation to study the performance of wind turbines: two-dimensional (2D) simulation and 3D simulation. 2D simulations are often used to investigate wind turbine parameters' impact on turbines' aerodynamic performance (Bianchini et al., 2017; Liang et al., 2017) due to their simple model and fewer computing resources. However, it ignores the flow field changes in the vertical distribution and assumes that the performance and characteristics of the turbines in the vertical direction are uniform. Therefore, it does not correspond to the real situation. By contrast, 3D simulations are much more realistic. They can capture 3D variations like the complex airflow disturbances and tip effects during turbine rotation (Azadani and Saleh, 2022; Kuang et al., 2022). Additionally, some studies have stated the differences between 2D and 3D simulations. They found that the differences in velocity magnitudes between these two simulation methods can reach about 10%, and the turbulent kinetic energy magnitudes in 2D simulations are significantly lower than that in 3D simulations (Lam and Peng, 2016; Bachant and Wosnik, 2016). Therefore, 3D simulations were chosen for the present research to ensure the rationality and authenticity of this study.

To address the limitations of previous research, this study simulated a pair of two-blade vertical-axis wind turbines positioned longitudinally under 3D modelling and considered the urban environment. Two arrangements were investigated: (1) both turbine 1 and turbine 2 set in a clockwise rotational direction, named C-C; (2) turbine 1 set in a clockwise rotational direction and turbine 2 set in a counter-clockwise rotational direction, named CO-C, to understand the aerodynamic effects and wind energy generation by turbines in a longitudinal arrangement, through analysing two typical parts of wake characteristics and power output (Vergaerde et al., 2020a).

2. Methods

2.1. Geometry model and grid arrangement

Figure 2 displays the computational domain and geometrical settings in the present study. The locations of boundary conditions: velocity-inlet, top, bottom, lateral, and pressure-outlet, were set at distances of 5 D, 5 D, 5 D, 4 D, and 11 D (with D being the diameter of the turbine) away from the turbines (Figure 2[a]). The vertical-axis wind turbine adopted in the present study has two blades, and each blade adopts a symmetrical straight blade with a NACA0021 (NACA, National Advisory Committee for Aeronautics; 0021, the parameter code of airfoil) airfoil shape, with the tip-speed ratio equal to 2.19. The diameter (D), height (H), and chord length of the turbine are 2 m, 1.2 m, and 0.265 m, and the swap area of the turbine is 2.4 m² (Figure 2[b]).

The sliding moving mesh method was utilised in the present study, and two cylindrical rotation regions were established to simulate the movement of wind turbines. The diameter and height of each rotation region were 1.5 times the diameter and the height of the turbine; additionally, the distance between the two turbines was set to 4 D (Figure 2[b]).

(a)

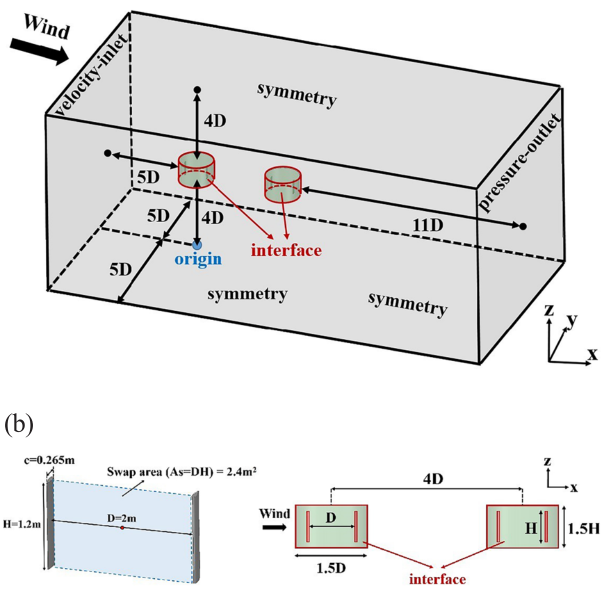

Figure 2. (a) Computational domain and boundary conditions; and (b) geometry model and dimensional settings of blades and two rotational regions.

The grid arrangement of the computational domain and near the blades is presented Figure 3. The minimum size of mesh at the surface of blades and rotational regions was set as 9 mm and 90 mm, respectively. The mesh growth rate was 1.15. The first-layer grid height near the blades was set to 0.039 mm to ensure the criterion of y+ < 5. The computational domain was discretised by tetrahedral cells, with a total grid number of 3,844,768 cells.

(a)

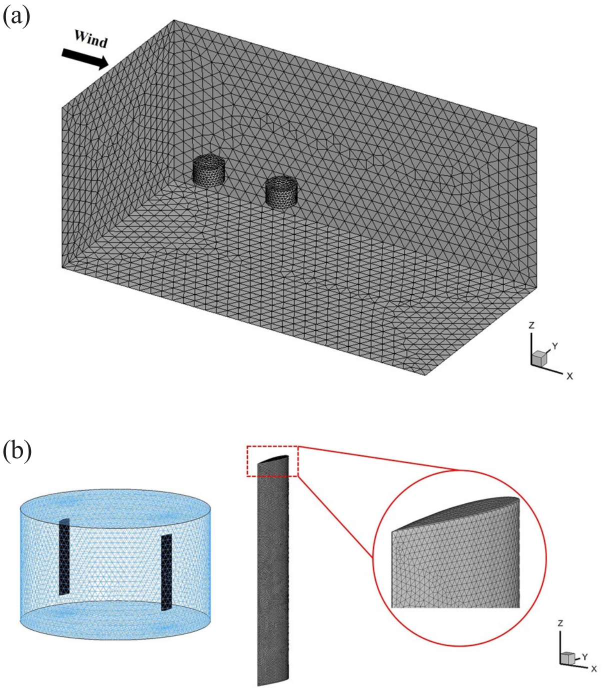

Figure 3. (a) Global mesh of computational domain; and (b) grid arrangement near the rotational regions and blades.

2.2. Boundary conditions and solver settings

Figure 2(a) shows the boundary conditions in the present study. Due to the vertical-axis wind turbines being placed on the roof and set at a certain height above the ground, it can be considered that they are less affected by the ground roughness; hence, the top, the bottom, the right side, and the left side of the domain were all set as symmetry conditions (Lam and Peng, 2016). The surfaces of the rotational regions were set as interface conditions, and all the surfaces of the blades were implemented in the no-slip boundary conditions.

In previous studies, a free mainstream wind speed was often used to simulate the incoming flow. However, in this study, a logarithmic wind profile was used to better reflect the effects of the surroundings and the topography. Considering the placement of wind turbines at a specific height above the ground and the influence of urban environments on turbines' performance, a segment of the logarithmic wind profile $U(z)$, dissipation rate (ω), and turbulent kinetic energy (k) was set within the inflow boundary conditions.

$$U(z) = \frac{u^*}{\kappa} ln \frac{z}{z_0}, \quad (1)$$

$$k = \frac{u^{*2}}{\sqrt{C_u}}, \quad (2)$$

$$\omega = \frac{u^{*3}}{\kappa(z+z_0)k}, \quad (3)$$

where z (m) is the height coordinate, $U(z)$ is the wind velocity at a height z, κ (=0.41) is the von Karman constant, and C_u (=0.09) is an empirical constant. z_0 (=0.5) is the aerodynamic roughness length, u^* (=0.68m/s) is the atmospheric boundary layer friction velocity, and they are fitted using the data obtained from Architectural Institute of Japan (AIJ) (Meng and Hibi, 1998). (z+30) means that only a section of wind profile above a height of 30 m above the ground was entered, and it was assumed that the height of the turbines was 4 m above the roof to ensure stability during movement. Additionally, in order to control variables, it was assumed that there were some approaches applied in the front of the buildings to reduce the flow separation, such as modifying the shape of building corners (Ye et al., 2024).

All the CFD simulations in the present research were implemented in the ANSYS Fluent 2022R1 commercial software package in Tianhe II. The RANS equations were applied to solve the 3D unsteady state for each case. The 4-equation transition SST turbulence model was applied as the closure model to fit the low Reynolds number flows near the wind turbine blades without any other wall functions introduced (Chen and Liou, 2011). The SIMPLE algorithm was used to solve the rotational movement of the wind turbine. The convergence criterion met the maximum requirement of residuals: 10^{-6} for continuity; 10^{-6}, 10^{-7}, and 10^{-9} for x velocity, y velocity, and z velocity, respectively. The time step size in the simulations was set to 0.000287 s (0.5°) – 0.000498 s (1°), and the maximum iteration for each time step was set to 30 to ensure converged results.

2.3. Validation and grid sensitivity analysis

The validation data in this study were derived from a previous wind tunnel test (Li et al., 2016). The vertical-axis wind turbine tested in this experiment has five blades and also adopts the NACA0021 airfoil shape, with a diameter (D) set to 2 m and a height (H) set to 1.2 m.

Three turbulence models, namely the realisable (RLZ) k-ε model, the 4-equation transition SST model (SST), and the Spalart-Allmaras (S-A) model, were tested to select the most appropriate one for further research. The average velocity from five lines along x/R = -1.8, -1.5, -1, -0.5, and 0 (upstream), and four lines along x/R = 0.5, 1, 1.5, and 2 (downstream) were selected for validation. Three metrics were used to evaluate the precision of the CFD results compared to the wind tunnel test (WT) results: FAC_2, FB, and R.

$$FAC_2 = \frac{1}{n}\sum_{i=1}^{n} n_i \quad with\ n_i \begin{cases} 1 & for\ 0.5 \leq \frac{P_i}{O_i} \leq 2 \\ 0 & else \end{cases}, \tag{4}$$

$$FB = \frac{2([P]-[O])}{[P]+[O]}, \tag{5}$$

$$R = \frac{\sum_{i=1}^{n}(P_i-\overline{P_0})(O_i-\overline{O_0})}{\sqrt{\sum_{i=1}^{n}(P_i-\overline{P_0})^2}\sqrt{\sum_{i=1}^{n}(O_i-\overline{O_0})^2}}, \tag{6}$$

where P_i and O_i are the data from the WT and CFD simulation, $\bar{P}_0$ and $\bar{O}_0$ are the average value for P_i and O_i, and n represents the number of data points. FAC_2 indicates the global accuracy of the CFD results. FB means the degree of under- or over-predictions in the CFD results. R represents the relevance between the WT and simulation results–its value is closer to 1–and the relevance between the two data sets is stronger.

Figure 4 displays the validation results at the upstream and downstream regions. These results are the average normalised velocity (U/U_{ref}) along the nine positions (x/R = -1.8, -1.5, -1, -0.5, 0, 0.5, 1, 1.5, and 2). It is evident that among these three models, the SST model's results show the best performance compared with the WT data, especially the results of the downstream region. The FB value of the SST model satisfies the acceptance criteria in both upstream and downstream regions and reaches the lowest value in the downstream region (Figure 4). Moreover, the R^2 value of the SST model is the closest to 1 among the three models (Table 1). Therefore, the SST model has the best performance in predicting the velocity field among these three models, and it was selected for further research.

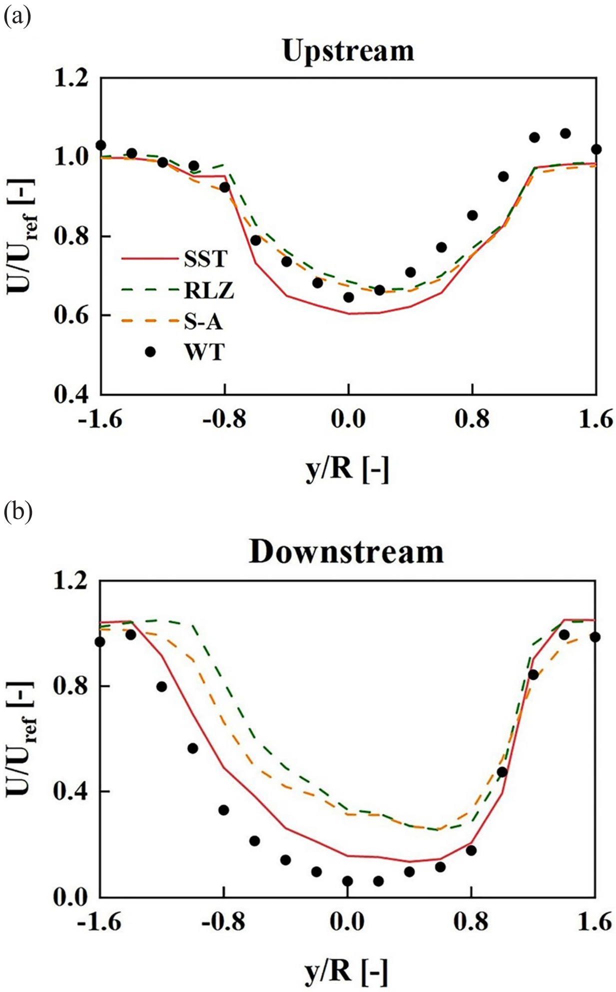

Figure 4. Validation results with different turbulence models at (a) upstream; and (b) downstream regions.

Table 1. Average errors for different turbulence models in the upstream and downstream regions: FAC_2, FB, and R^2.

Validations metrics		FAC_2	FB	R^2
Upstream	SST	1	0.06	0.93
	Realisable	1	0.04	0.87
	S-A	1	0.29	0.90
Downstream	SST	1	-0.31	0.99
	Realisable	1	-0.60	0.92
	S-A	1	-0.55	0.96

The SST turbulence model was used to conduct the simulation of grid sensitivity analysis. Three grids with different grid numbers were tested: coarse (3,196,086 cells), medium (4,805,032 cells), and fine (6,108,963 cells), and the grid refinement ratio was set to $\sqrt{2}$. The independency of the grid number was evaluated via the grid convergence index (GCI) (Roache, 1997):

$$GCI = f_s \left| \frac{r^p (U_{i,a} - U_{i,b}) / U_{ref}}{1 - r^p} \right|, \quad (7)$$

where p (=2) is the order of accuracy, f_s is the safety constant taken at 1.25, and r is the grid refinement set to $\sqrt{2}$. $U_{i,a}$ and $U_{i,b}$ are the velocity values in two sets of data, and U_{ref} is the reference velocity.

As shown in Figure 5, little difference is shown in the results of these three grids, in predicting the velocity field of both upstream and downstream regions Figures 5(a) and 5(b). The results of GCI between the coarse and medium grids and the maximum values of GCI for the upstream and downstream regions are both not more than 3% (Figures 5[c] and 5[d]). This demonstrates that there is a relative independence between the number of grids and the existing grid division which can guarantee the accuracy of the numerical solution. Considering the computational time cost during the simulation, the coarse grid was adopted for the present research.

(a)

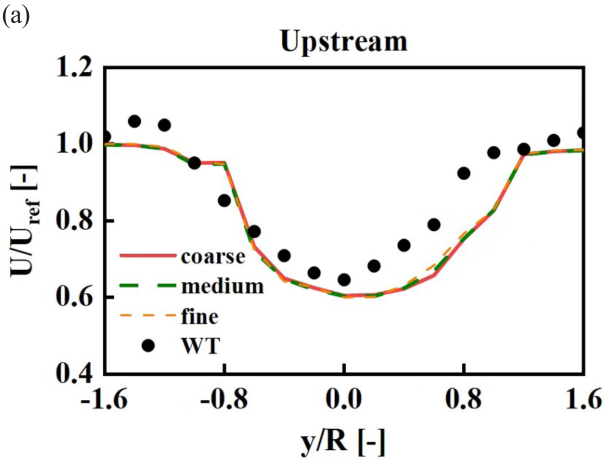

(b)

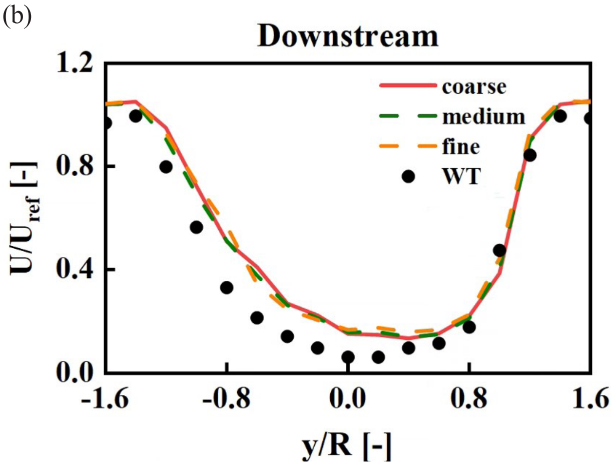

(c)

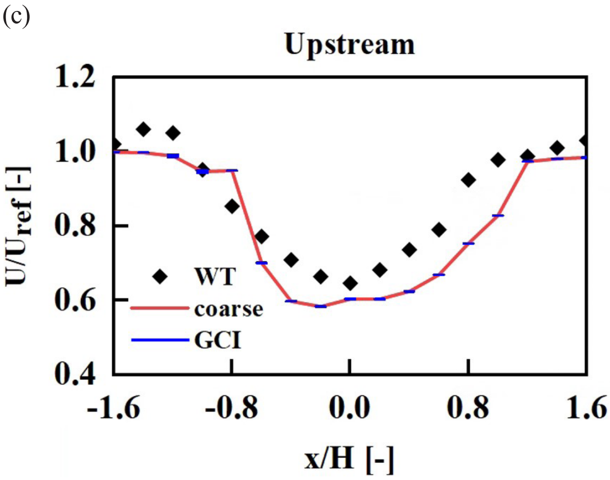

(d)

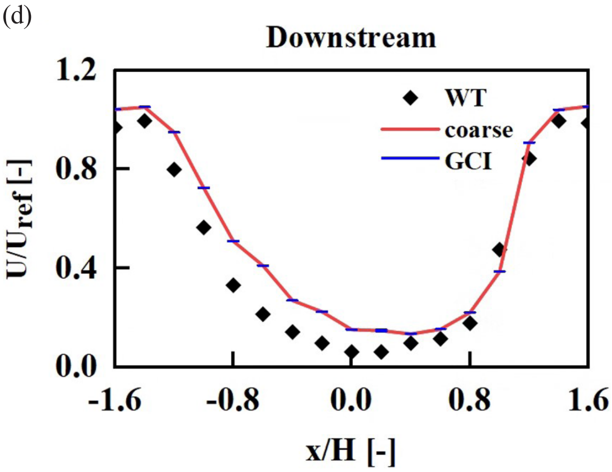

Figure 5. Grid sensitivity analysis results for coarse, medium, and fine grids at (a) upstream; and (b) downstream regions. The coarse grid with GCI: (c) upstream; and (d) downstream.

3. Results and discussion

The wake characteristics for two cases of C-C and CO-C at the horizontal centre plane (z - 4D)/H = 0.5 are shown in Figure 6. Due to turbine 1 having the opposite rotational direction in two cases, the wake characteristics between turbine 1 and turbine 2 present different patterns of biases. In the case of C-C, the wake biases towards the positive y direction, and its larger velocity deficit biases towards the positive y direction (Figure 6[a], Line 1). Similarly, the wake in the CO-C case biases towards the negative y direction, and the larger deficits are also found in this direction (Figure 6[b], Line 2). The wake of turbine 1 caused by the opposite rotational directions may result in different impacts on the power output and velocity deficits of turbine 2. The wake length in the C-C case is longer, and its range of U/U_{ref} is less than 0.25, which is significantly larger than that of the CO-C. This is because the same rotational direction between turbine 1 and turbine 2 makes the wake behind the turbines prone to superpose in the same direction, thus causing more significant wake deficits and longer wake lengths.

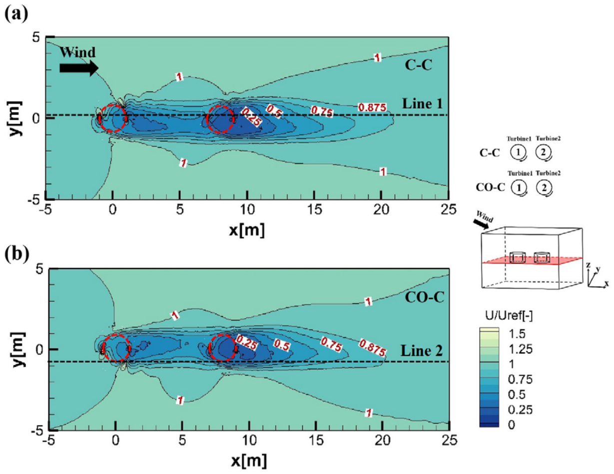

Figure 6. Distribution of U/U_{ref} (U_{ref} = 8 m/s) at the horizontal centre plane (z-4D)/H = 0.5 for (a) C-C; and (b) CO-C.

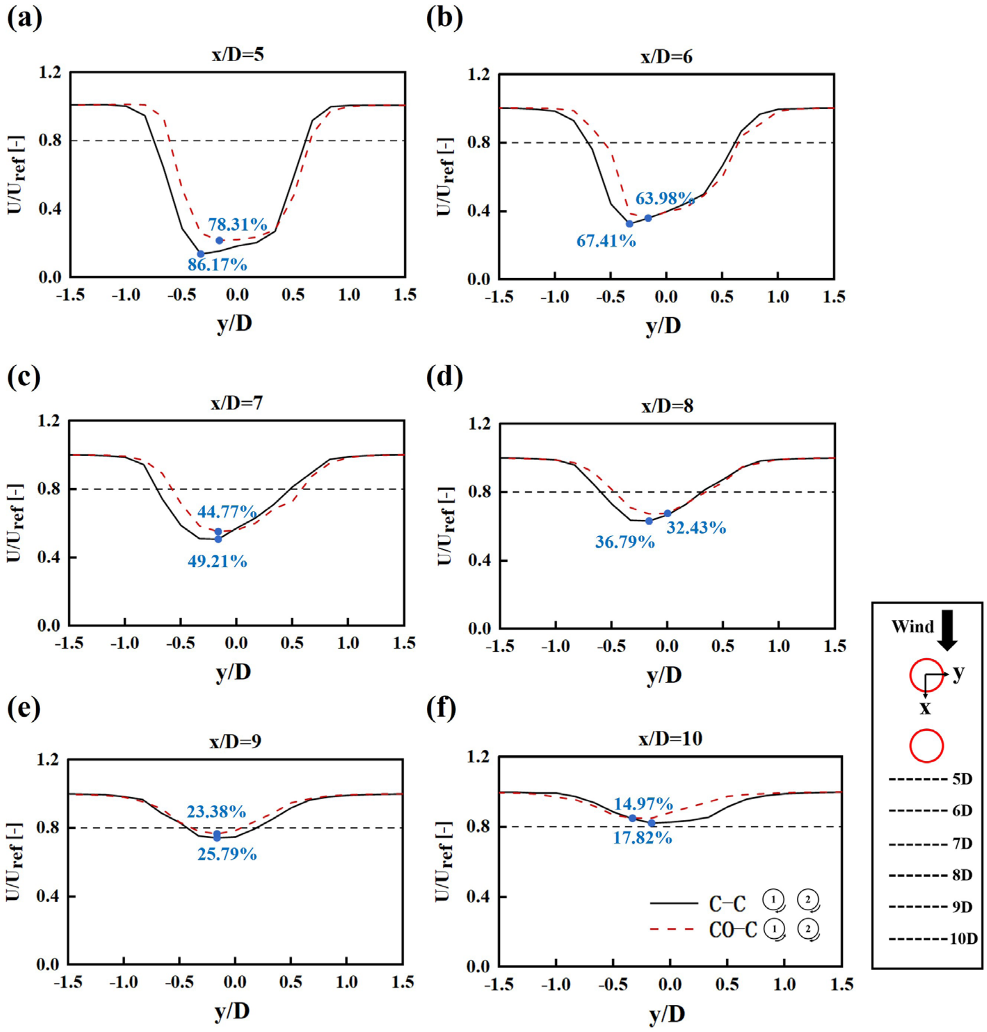

Figure 7. Velocity deficits for C-C and CO-C along six lines: (a) x/D = 5; (b) x/D = 6; (c) x/D = 7; (d) x/D = 8; (e) x/D = 9; and (f) x/D = 10.

Figure 7(a) displays the locations of six horizontal lines (x/D = 5, 6, 7, 8, 9, and 10) selected to quantify the velocity deficits. Figures 7(b) to 7(f) display the results of deficits for C-C and CO-C along these six lines. The maximum value occurs at x/D = 5 both for C-C and CO-C. The maximum deficit of C-C is 86.17%, and that of CO-C is 78.31%, which is about 10% lower than that of C-C. The deficits of C-C at lines of x/D = 6, 7, 8, 9, and 10 are also larger than that of CO-C. So, it can be demonstrated that, due to the influence of the superposition effects, two longitudinally arranged turbines with the same rotational direction indeed cause larger wake deficits than those rotating in opposite directions. Note that before x/D = 8, the wake pattern of C-C shows asymmetry and biases towards the negative y direction due to the influence of the clockwise direction. At x/D = 9, because the impact of the turbines' movement becomes much lower and the wake deficit recovers intensively with increasing downstream distance, the wake patterns show symmetry. The wake velocity of C-C recovers at least 80% (Lam and Peng, 2016) at x/D = 10, located at 5.5 D behind turbine 2. For the case of CO-C, before x/D = 8, due to the influence of the counter-clockwise rotation of turbine 1, the wake velocity behind turbine 2 presents a lighter bias towards the negative y direction. At x/D = 9, the wake behind turbine 2 shows symmetry, which presents the same feature as the case of C-C. At x/D = 10, it is significant that the wake biases towards the positive y direction achieve a faster recovery; this is because in the case of CO-C, turbine 1 and turbine 2 have the opposite rotational direction, so the superposition degree of velocity deficits is lighter behind turbine 2. The rotational direction of turbine 2 is clockwise, so the wake deficit mainly biases toward the negative y direction; thus, the deficits generated in a positive y direction can achieve a faster recovery. Moreover, the wake velocity also recovers at least 80% (Lam and Peng, 2016) at x/D = 10 in the scenario of CO-C. This means that the turbines placed behind turbine 2 must be positioned at least 5.5 D downstream to obtain a sufficiently high incoming wind speed.

Figures 8(a) and 8(b) display the velocity fields at the vertical plane y/D = 0. The distributions of wake deficits in the C-C and CO-C cases exhibit symmetry on the vertical plane. However, the wake length of C-C is longer than that of CO-C, consistent with the results presented in Figure 6. The results show that varying degrees of velocity deficits still exist at a certain distance downstream in the vertical plane. At the height of $H^{0.5}$, the wake velocity reaches the maximum deficit value of 49.20% and 44.76% for C-C and CO-C respectively. With the increases and decreases in height, the degree of wake deficit begins to become smaller, but its value is still more than 20% at the lowest height of H_0 and highest height of H^1, both for the C-C and CO-C cases. This demonstrates that, in the vertical direction, there is still a significant velocity deficit at a certain downstream distance behind the turbines, and these wake deficits may impact the surrounding flow field. The 2D simulation could not reflect this vertical variation and provide an oversight of the influence of wake deficits on the surrounding environment. However, the 3D simulation can present these changes and characteristics more objectively.

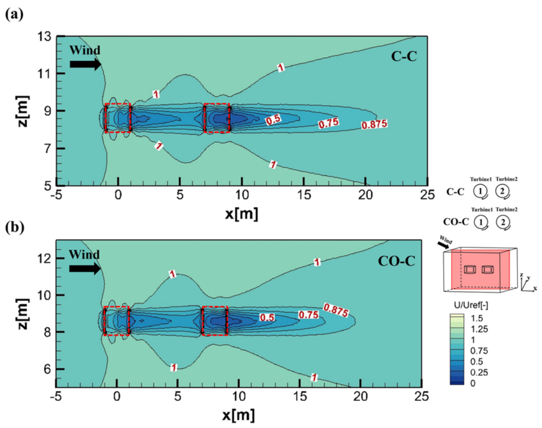

Figure 8. Distribution of U/U_{ref} (U_{ref} = 8 m/s) at vertical centre plane y/D = 0 for (a) C-C; (b) CO-C.

The Cp is a vital indicator to evaluate the wind power generating capacity of turbines, by calculating the following function (Vergaerde et al., 2020b):

$$Cp = \frac{\tau\lambda}{0.5\rho V^2 R A_S}, \quad (8)$$

where τ is the torque during the wind turbines' movement, R is the radius of the turbines, V is the reference velocity, λ represents the tip-speed ratio, ρ is the air density, and A_s is the swap area.

Figure 9 displays the Cp curves of turbine 1 and turbine 2 for the cases of C-C and CO-C. As Figure 9(a) shows, due to no other resistance before turbine 1, the Cp of turbine 1 in the two cases show no significant differences even though its rotational direction has changed. However, the dynamics of turbine 1 impact the power output of turbine 2. As shown in Figure 9(b), the Cp of C-C and CO-C present different wave patterns. The low value of fluctuation in CO-C is lower than that of C-C; this demonstrates that the opposite rotational direction of turbine 1 and turbine 2 can cause a lower Cp of turbine 2 in some orientations, thus generating a lower power output from two turbines. Even though the degree of wake velocity deficits in C-C is larger, it seems to generate a higher power output due to the acceleration in the same rotational direction. The average Cp of turbine 1 in C-C and CO-C is 27.41% and 27.12% respectively, and the Cp of turbine 2 in C-C is 2.09% and in CO-C is less than zero. In the case of C-C, the average Cp of turbine 2 is about 92.37% lower than that of turbine 1. This demonstrates that the turbine located upstream significantly impacts the downstream turbine's power output. However, comparing the two longitudinal arrangements of C-C and CO-C, the generated capacity of C-C is higher than that of CO-C, which means that the same rotational direction of turbines with a longitudinal arrangement could generate a larger power output than those with the opposite rotational direction.

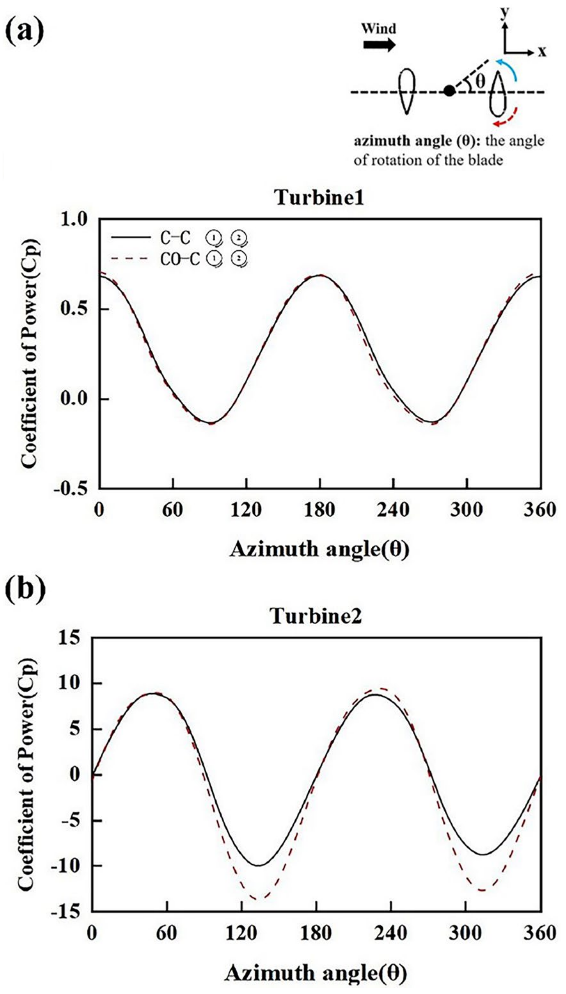

Figure 9. The *Cp* of C-C and CO-C for (a) turbine 1; and (b) turbine 2.

4. Limitation of this study

This study explored the interactions and generating capacity of a pair of vertical-axis wind turbines with a longitudinal arrangement in an urban environment. However, some limitations still deserve attention.

First, the blades of vertical-axis wind turbines are an important factor affecting the generation capacity of turbines. However, in this paper, only one type of airfoil shape was considered. It is also important to analyse different airfoil types' impact on the power output in further research.

Second, in an urban environment, the layout and shape of the surrounding buildings are also important factors affecting the flow fluctuations around the wind turbines. In order to study the performance of the turbines more specifically, the building models were simplified in this study. However, in the actual situation, the buildings' impacts and the flow separation that they cause are worth further consideration.

The study of wind turbine arrays is an important aspect. In this study, only the performance of a basic unit was simulated, namely two wind turbines with a longitudinal arrangement. It is worth further exploring the performance of multiple turbines with different parameter settings and putting forward more practical design schemes.

5. Conclusion

The present paper explores the interactions and generating capacity of a pair of vertical-axis wind turbines with a longitudinal arrangement, considering the wind direction with a 0-degree wind attack angle and the boundary conditions with the characteristics of urban environments. Below are the main conclusions of this study.

The maximum wake deficit value and wake length for C-C are greater than for CO-C. This implies that the co-rotation of the wind turbines has more pronounced actions on wake superposition and wake deficit.

Both in C-C and CO-C cases, the wake velocity can recover 80% at a distance of 5.5 D behind turbine 2. The next turbine should be placed at least at this distance to ensure enough inflow velocity.

In the vertical direction, a significant wake deficit still exists at a certain distance behind the wind turbines in both the C-C and CO-C cases. This demonstrates the significance of studying vertical wake deficits and the necessity of employing 3D simulations.

The longitudinal arrangement of C-C can generate a larger power output than that of CO-C. The longitudinal arrangement of C-C should be prioritised to explore larger power outputs of urban wind energy.

Acknowledgement

This study was supported by the National Natural Science Foundation of China (No. 42175180 and 21EAA00654), the Guangdong Province Key Laboratory for Climate Change and Natural Disaster Studies (No. 2020B1212060025), and the Innovation Group Project of Southern Marine Science and Engineering Guangdong Laboratory (No. 311020001). The CFD simulations of this research were conducted on the Tianhe II supercomputer at the National Supercomputer Center, Guangzhou, People's Republic of China .

Notes on contributors

Dr Xuelin Zhang is currently an Associate Professor attached to the School of Atmospheric Sciences at Sun Yat-sen University (SYSU), and she is the Principle Investigator (PI) of Future City-BEUP (Built Environment and Urban Physics) Lab. Her current research focuses on urban wind and thermal environments, natural ventilation, air pollutant dispersion, aerosol dispersion, built wind energy, novel building forms, and machine learning applications in environmental wind engineering. In addition, she is serving as an associate editor of Physics of Fluids (JCR Q1 Top), a reviewer for several international journals and a committee member of National Key Laboratory of Atmospheric Physics Simulation and Pollution Control.

Miss Xiulan Ye is a master's student supervised by Dr Xuelin Zhang at the School of Atmospheric Sciences, Sun Yat-sen University. Her research focuses on wind energy resources in urban environments. She works to optimise building roof design through CFD simulation and machine learning to enhance wind energy harvesting from roof-mounted wind turbines.

Miss Lin Wen is a master's student at the School of Atmospheric Sciences at Sun Yat-sen University. Her current main research focus is dynamic mesh method, urban wind energy, wind turbine layouts, and traffic pollution in urban environments.

References

[1] Abohela I, Hamza N and Dudek S (2013). Effect of roof shape, wind direction, building height and urban configuration on the energy yield and positioning of roof mounted wind turbines. *Renewable Energy*, 50, pp. 1106–1118. https://doi.org/10.1016/j.renene.2012.08.068

[2] Azadani LN and Saleh M (2022). Effect of blade aspect ratio on the performance of a pair of vertical axis wind turbines. *Ocean Engineering*, 265, pp. 112627. https://doi.org/10.1016/j.oceaneng.2022.112627

[3] Balduzzi F, Bianchini A and Ferrari L (2012). Microeolic turbines in the built environment: Influence of the installation site on the potential energy yield. *Renewable Energy*, 45, pp. 163–174. https://doi.org/10.1016/j.renene.2012.02.022

[4] Bachant P and Wosnik M (2016). Modeling the near-wake of a vertical-axis cross-flow turbine with 2-D and 3-D RANS. *Journal of Renewable and Sustainable Energy*, 8, pp.053311. https://doi.org/10.1063/1.4966161

[5] Bianchini A, Balduzzi F, Bachant P, Ferrara G and Ferrari L (2017). Effectiveness of two-dimensional CFD simulations for Darrieus VAWTs: a combined numerical and experimental assessment. *Energy Conversion and Management*, 136, pp. 318–328. https://doi.org/10.1016/j.enconman.2017.01.026

[6] Brownstein ID, Kinzel M and Dabiri JO (2016). Performance enhancement of downstream vertical-axis wind turbines. *Journal of Renewable and Sustainable Energy Reviews*, 8, 053306. https://doi.org/10.1063/1.4964311

[7] Chen TY and Liou LR (2011). Blockage corrections in wind tunnel tests of small horizontal-axis wind turbines. *Experimental Thermal and Fluid Science*, 35, pp. 565–569. https://doi.org/10.1016/j.expthermflusci.2010.12.005

[8] Hassanli S, Hu G, Kwok KCS and Fletcher DF (2017). Utilizing cavity flow within double skin façade for wind energy harvesting in buildings. *Journal of Wind Engineering and Industrial Aerodynamics*, 167, pp. 114–127. https://doi.org/10.1016/j.jweia.2017.04.019

[9] Huang P, Peng X and Gu M (2017). Wind tunnel study on effects of various parapets on wind load of a flat-roofed low-rise building. *Advances in Structural Engineering*, 20, pp. 1907–1919. https://doi.org/10.1177/1369433217700425

[10] Juan YH, Rezaeiha A, Montazeri H, Blocken B, Wen CY and Yang AS (2022). CFD assessment of wind energy potential for generic high-rise buildings in close proximity: Impact of building arrangement and height. *Applied Energy*, 321, pp. 119328. https://doi.org/10.1016/j.apenergy.2022.119328

[11] Kuang L, Lu Q, Huang X, Song L, Chen Y, Su J, Han Z, Zhou D, Zhao Y, Xu Y and Liu Y (2022). Characterization of wake interference between two tandem offshore floating vertical-axis wind turbines: Effect of platform pitch motion. *Energy Conversion and Management*, 265, pp. 115769. https://doi.org/10.1016/j.enconman.2022.115769

[12] Lam HF and Peng HY (2016). Study of wake characteristics of a vertical axis wind turbine by two- and three-dimensional computational fluid dynamics simulations. *Renewable Energy*, 90, pp. 386–398. https://doi.org/10.1016/j.renene.2016.01.011

[13] Lam HF and Peng HY(2017). Measurements of the wake characteristics of co- and counter-rotating twin H-rotor vertical axis wind turbines. *Energy*, 131, pp. 13–26. https://doi.org/10.1016/j.energy.2017.05.015

[14] Li Q, Maeda T, Kamada Y, Murata J, Furukawa K and Yamamoto M (2016). Measurement of the flow field around straight-bladed vertical axis wind turbine. *Journal of Wind Engineering and Industrial Aerodynamics*, 151, pp. 70–78. https://doi.org/10.1016/j.jweia.2016.01.012

[15] Liang X, Fu S, Ou B, Wu C, Chao CYH and Pi K (2017). A computational study of the effects of the radius ratio and attachment angle on the performance of a Darrieus-Savonius combined wind turbine. *Renewable Energy*, 113, pp. 329–334. https://doi.org/10.1016/j.renene.2017.04.071

[16] Meng Y and Hibi K (1998). Turbulent measurments of the flow field around a high-rise building. *Wind Engineers, JAWE*, 1998, pp. 55–64. https://doi.org/10.5359/jawe.1998.76_55

[17] Müller S, Muhawenimana V, Wilson CAME and Ouro P (2021). Experimental investigation of the wake characteristics behind twin vertical axis turbines. *Energy Conversion and Management*, 247, pp. 114768. https://doi.org/10.1016/j.enconman.2021.114768

[18] Raciti Castelli M, Englaro A and Benini E (2011). The Darrieus wind turbine: Proposal for a new performance prediction model based on CFD. *Energy*, 36, pp. 4919–4934. https://doi.org/10.1016/j.energy.2011.05.036

[19] Rezaeiha A, Montazeri H and Blocken B (2018). Characterization of aerodynamic performance of vertical axis wind turbines: Impact of operational parameters. *Energy Conversion and Management*, 169, pp. 45-77. https://doi.org/10.1016/j.enconman.2018.05.042

[20] Rezaeiha A, Montazeri H and Blocken B, (2020). A framework for preliminary large-scale urban wind energy potential assessment: Roof-mounted wind turbines. *Energy Conversion and Management*, 214, pp. 112770. https://doi.org/10.1016/j.enconman.2020.112770

[21] Roache PJ (1997). QUANTIFICATION OF UNCERTAINTY IN COMPUTATIONAL FLUID DYNAMICS. *Annual Review of Fluid Mechanics*, 29, pp. 123–160. https://doi.org/10.1146/annurev.fluid.29.1.123

[22] Škvorc P and Kozmar H (2021). Wind energy harnessing on tall buildings in urban environments. *Renewable and Sustainable Energy Reviews*, 152, pp. 111662. https://doi.org/10.1016/j.rser.2021.111662

[23] Toja-Silva F, Colmenar-Santos A and Castro-Gil M (2013). Urban wind energy exploitation systems: Behaviour under multidirectional flow conditions-Opportunities and challenges. *Renewable and Sustainable Energy Reviews*, 24, pp. 364–378. https://doi.org/10.1016/j.rser.2013.03.052

[24] Vergaerde A, De Troyer T, Muggiasca, S, Bayati I, Belloli M, Kluczewska-Bordier J, Parneix N, Silvert F and Runacres MC (2020a). Experimental characterisation of the wake behind paired vertical-axis wind turbines. *Journal of Wind Engineering and Industrial Aerodynamics*, 206, pp. 104353. https://doi.org/10.1016/j.jweia.2020.104353

[25] Vergaerde A, De Troyer T, Standaert L, Kluczewska-Bordier J, Pitance D, Immas A, Silvert F and Runacres MC (2020b). Experimental validation of the power enhancement of a pair of vertical-axis wind turbines. *Renewable Energy*, 146, pp. 181–187. https://doi.org/10.1016/j.renene.2019.06.115

[26] Xu W, Li G, Zheng X, Li Y, Li S, Zhang C and Wang F (2021a). High-resolution numerical simulation of the performance of vertical axis wind turbines in urban area: Part I, wind turbines on the side of single building. *Renewable Energy*, 177, pp. 461–474. https://doi.org/10.1016/j.renene.2021.04.071

[27] Xu W, Li Y, Li G, Li S, Zhang C and Wang F (2021b). High-resolution numerical simulation of the performance of vertical axis wind turbines in urban area: Part II, array of vertical axis wind turbines between buildings. *Renewable Energy*, 176, pp. 25–39. https://doi.org/10.1016/j.renene.2021.05.011

[28] Ye X, Zhang X, Weerasuriya AU, Hang J, Zeng L and Li CY (2024). Optimum design parameters for a venturi-shaped roof to maximize the performance of building-integrated wind turbines. *Applied Energy*, 355, pp. 122311. https://doi.org/10.1016/j.apenergy.2023.122311

[29] Zanforlin S and Nishino T (2016). Fluid dynamic mechanisms of enhanced power generation by closely spaced vertical axis wind turbines. *Renewable Energy*, 99, pp. 1213–1226. https://doi.org/10.1016/j.renene.2016.08.015

[30] Zhou H, Lu Y, Liu X, Chang R and Wang B (2017). Harvesting wind energy in low-rise residential buildings: Design and optimization of building forms. *Journal of Cleaner Production*, 167, pp. 306–316. https://doi.org/10.1016/j.jclepro.2017.08.166